# Binary Synergy Strengthening and Toughening of Bio-Inspired Nacre-like Graphene Oxide/Sodium Alginate Composite Paper

Ke Chen, Bin Shi, Yonghai Yue,* Juanjuan Qi, and Lin Guo*

Key Laboratory of Bio-inspired Smart Interfacial Science and Technology of Ministry of Education, School of Chemistry and Environment, Beihang University, Beijing 100191, People's Republic of China

ABSTRACT A crucial requirement for most engineering materials is the excellent balance of strength and toughness. By mimicking the hybrid hierarchical structure in nacre, a kind of nacre-like paper based on binary hybrid graphene oxide (GO)/sodium alginate (SA) building blocks has been successfully fabricated. Systematic evaluation for the mechanical property in different (dry/wet) environment/after thermal annealing shows a perfect combination of high strength and toughness. Both of the parameters are nearly many-times higher than those of similar materials because of the synergistic strengthening/toughening enhancement from the binary GO/SA hybrids. The successful fabrication route offers an excellent approach to design advanced strong integrated nacre-like composite materials, which can be applied in tissue engineering, protection, aerospace, and permeable membranes for separation and delivery.
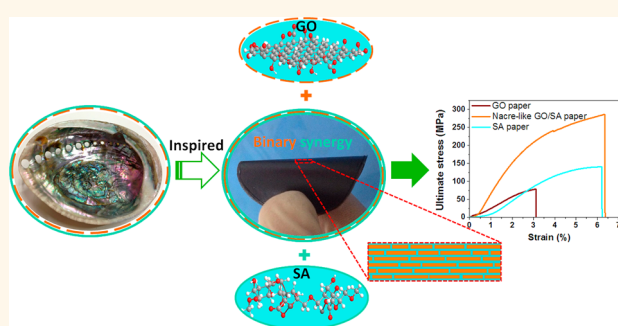
KEYWORDS: bio-inspired · artificial nacre · mechanical properties · binary synergy · graphene oxide · sodium alginate

During the long evolutionary process, nature uses its own ingenious and magical ways to produce lightweight, strong, and tough materials with complex, hierarchical architecture.[1−4] Current natural materials such as cellulose tissues,[5,6] collagen tissues,[7] mineralized tissues,[4] and nacre (mother-of-pearl)[8,9] have captured special attention in material science[10] because of their light weight, exceptional mechanical and other properties, and huge potential capacity to enhance the mechanical performance of conventional pure/simple materials.[11] One of the most popular biological models is the "bricks-and-mortar" arrangement of nacre, which contains inorganic and organic constituents.[12] The precise arrangement constituted of well-aligned inorganic 2D platelets surrounded by an elastic biopolymer matrix plays a critical role in the combination of excellent strength and toughness in nacre.[3] Based on the excellent nacre model, different types of inorganic materials have been utilized as reinforcing platelets to fabricate

polymer matrix artificial composites, including alumina,[9] graphene,[11,13,14] graphene oxide (GO),[2,15−18] clay,[1,19,20] and flattened carbon nanocubes.[21] So far, although great progress has been achieved in mechanical properties by using the 2D platelet,[22,23] only a few of these artificial laminar composites possess both strength and toughness.[3]

The selection of an ideal reinforcing platelet and polymetric matrix, which can effectively transfer loading, plays a key role in the achievement of both high strength and toughness.[2,20] Here, GO and sodium alginate (SA) were elected as the candidates to fabricate these new composites. Individual GO sheets have been verified as an ideal reinforcing filler because of their light weight, outstanding mechanical properties (Young's modulus up to 250 GPa), high aspect ratio (~1 nm thick × 2.5−5 μm diameter sheets), high flexibility, good ductility, and superior processability.[24] In addition, GO sheets consist of a hexagonal carbon network with both sp[2]- and sp[3]-hybridized carbons possessing a multitude of oxygen-containing functional

groups on its "basal" surface, which further improve the interfacial interactions with the polymer matrix by numerous H-bonding networks.[25] Natural biomaterials can be considered to be ideal candidates for polymeric matrices due to a series of merits such as being easily obtainable, environmentally friendly, and mechanically outstanding.[4,26,27] Sodium alginate, a kind of linear anionic polysaccharide copolymer, consists of two different repeating units possessing massive oxygen-containing functional groups (−OH, −COO, and −O−), where the material is water-like in its H-bonding ability, and there will be strong covalent bonds between the H-bonding-capable repeating units.[26,28] Besides, in terms of molecular design, the molecular structure of SA is more similar to that of the chitin in the organic phase of natural nacre.

In this work, we designed a new artificial nacre-like composite paper by vacuum-assisted flocculation (VAF) of GO/SA hybrid building blocks (Figure 1). It is worth mentioning that the values of the mechanical properties obtained in the natural environment (25 °C, 15% relative humidity (RH)) are many-fold higher than that of previous materials (such as several types of natural materials or composites containing SA biopolymer with different fillers or different polymeric materials with GO sheets). A unique combination of high ultimate stress (272.3 ± 13.9 MPa) and high toughness (12.5 MJ m^{-3}, up to 18.1 ± 0.6 MJ m^{-3} in some cases) for our composite paper has been achieved. The strong cooperative/H-bonding interactions between both components, which have abundant oxygen-containing functional groups on their interfaces, are supposed to be responsible for the binary synergistic strengthening/toughening enhancement. Besides, this GO/SA composite paper also has excellent mechanical performance in the natural environment or below 70 °C with low RH. The successful fabrication route offers an outstanding method to design and process advanced strong integrated nacre-like composite materials, which can be applied in tissue engineering, protection, aerospace, and permeable membranes for separation and delivery.

RESULTS AND DISCUSSION

To assemble the nacre-like GO/SA composite paper, GO was first oxidized from a natural graphite flakes by a modified Hummers method.[15,25,29,30] The Raman spectrum of GO sheets shows that the D band at approximately 1355 cm^{-1} and the G band located at 1593 cm^{-1}, with a ratio of integrated peak intensities of $I_D/I_G = 1.5$, are consistent with the previous results (Supporting Information (SI), Figure S1a).[31,32] Then, GO underwent complete exfoliation in water, yielding colloidal suspensions of almost entirely individual GO sheets with a mean lateral dimension of approximately 2.5 μm and a thickness of about 0.96 nm (Figure S1b). As shown in Figure 1, using SA as an ideal matrix to
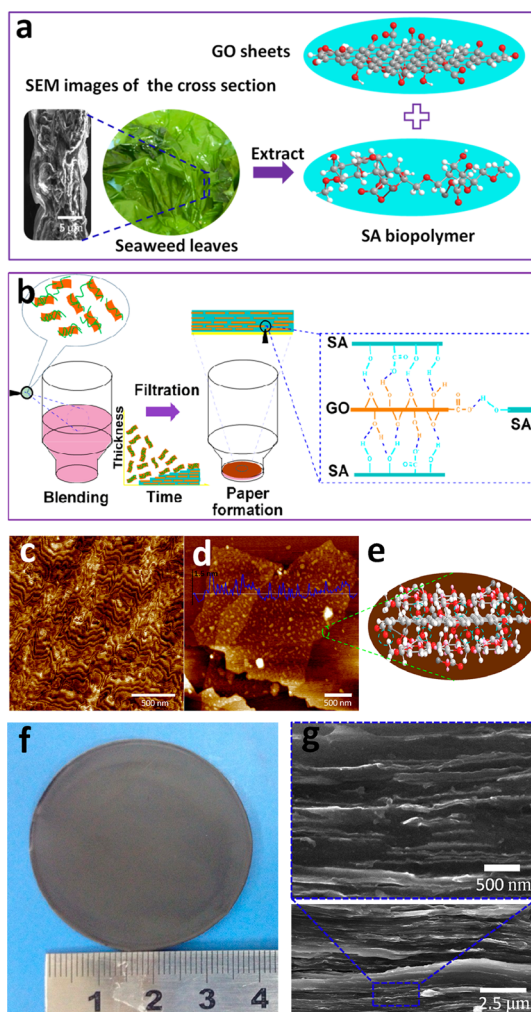
Figure 1. (a) Molecular models of GO sheets and SA biopolymer. **(b)** Fabrication process of artificial nacre-like composite paper. From left to right: Individual GO sheets easily absorbed SA biopolymer on their surfaces as building blocks are successfully assembled by VAF. Proposed structural model, in which GO sheets are regularly embedded into the SA matrix to form the layered structure. The interaction between two components is generally regarded as multiple hydrogen bonds. **(c)** Atomic force microscopy images of the morphology of the hybrid GO/SA membrane. **(d)** Topography (Z-scale: 12.4 nm) of the GO/SA hybrid structure deposited on top of a mica sheet. SA biopolymer absorption on GO sheets (Z-range: 13.3 nm). The height profile of the cross section shows that the thickness (~2.0 nm) of GO-sheet-absorbed SA can be attributed to the biopolymer on (and underneath) the GO sheet; the root mean square (rms) roughness is about 0.87 nm within 1.5 μm × 1.5 μm surface area. **(e)** Molecular models of the H-bonding interactions (broken circles) on the interface between GO sheets (middle) and SA biopolymer (top and bottom). **(f)** Digital photograph of the nacre-like composite paper. **(g)** Cross-sectional morphology of the nacre-like composite paper. Note: elements in the ball-and-stick model of (a) and (e) are differently color coded: H, white; C, light gray; O, red; Na, dark gray; lone pair, pink.

form the ball-and-stick model (Figure 1a), the colloidal GO suspension was blended into aqueous SA solution to fabricate the composite paper by VAF (Figure 1b). The color of the blends changed gradually from transparent to brown as the GO content increased, and the

blend with 18.6 vol % of GO showed no agglomeration (Figure S2a) and decreased for the transmission (Figure S2b) even after 2 months. Change of GO content can be easily monitored by UV−vis spectroscopy, as shown in Figure S2c.[33] The absence of agglomerations indicated that the attractive cooperative interactions between these two components should be dispersive attractions (e.g., H-bonding, van der Waals). Atomic force microscopy (AFM) imaging demonstrates that the topography of the hybrid GO/SA membrane is relatively uniform with a root mean square (rms) roughness of 1.53 ± 0.05 nm within 5.0 μm $\times$ 5.0 μm, based on the analytical results in Figure 1c and Figure S2d$_{s1,s2}$. Furthermore, as shown in Figure 1d and Figure S2d$_{s3}$, the multidomain morphology of SA biopolymer macromolecules uniformly distributed on the surface of the GO sheet is shown in the high-resolution AFM. The average thickness of an absorbed layer of SA biopolymer is ~0.25 nm if taking away the thickness of the GO sheets (~1 nm) (see Figure 1d andSupporting Information Figure S2d$_{s3,s3i}$). Furthermore, the surface density of the adsorbed SA biopolymers on GO sheets is obviously higher than those on the mica surface, suggesting strong cooperation of two components after efficacious absorption from SA solution during fast solvent evaporation.[2] Higher density of oxygen-containing functional groups results in an increased network of H-bonding. The H-bond network is primarily dominated not only by the bonds between the oxygen-containing functional groups of these two components but also by the bonds between water molecules and oxygen-containing functional groups. Therefore, it is the cooperative interactions, the driving force to form a strong hybrid surface (Figure 1e), which ensure the efficient load transfer from the SA matrix to the GO sheets.[20,23] Additionally, rather than bundles of lignocellulose as normally observed for time-consuming absorption on hydrophilic substrates, SA biopolymer macromolecules are easily dispersed in water to form amorphous microstructures, which are similar to silk fibers or other biopolymers. Hence, due to the absence of significant aggregation of the GO/SA blend, interfacial interactions between oxygen-containing groups of GO sheets and SA domains are present. Finally, the well-aligned composite paper can be easily obtained by accurately controlling the GO concentration at 18.6 vol %, and the thickness increases linearly with the volume of blend solution (Figure 1f,g and Figure S2e in SI).

The cross-sectional morphologies of the composite papers with different GO concentration have been checked by scanning electron microscopy (SEM) (Figure 2a−d and Figure S3 in SI). As shown in Figure 2a, the SA paper with packed and unshaped tactoid is considered to be one unit layer, and the laminated structure of the composite can be distinguished clearly with the increment of GO concentration.

When the GO concentration is ~18.6 vol %, the composite paper exhibits a laminated structure with well-aligned platelets with ~50 nm thickness surrounded by the SA matrix. With the GO concentration further increasing (greater than 25.5 vol %), GO sheets will interpenetrate into adjacent SA layers to form an intercalated, densely packed, "wavy" layered heterostructure, which is similar to that of the less densely packed "wavy" layer of GO (Figures 2c,d and S3c−h and S4 in SI).

Fourier transform infrared (FTIR) image displays the bands centered at 1740 and 1230 cm^{-1}, showing the gradually decreased C═O and C−O stretch intensities, the peak at 1230 cm^{-1} shifted to the higher wavenumbers of 1290 cm^{-1}, the peaks centered at 1620 and 1400 cm^{-1} exhibiting gradually increased C═C and C−O stretch intensities, and the peak at 1620 cm^{-1} shifted to the lower wavenumbers at 1590 cm^{-1} (Figure 2e). The results mentioned above indicate that GO sheets indeed attached to the SA biopolymer and can be regarded as a proof of the H-bonding between C═O or C−O and OH, agreeing well with the observed increase of the OH band. The two bands centered around 1050 and 1100 cm^{-1} in the SA biopolymer, corresponding to O−C═O and C−O stretching, increased in intensity by 80 and 60 cm^{-1} in the composite papers, in comparison with those of neat GO paper, respectively. In contrast to the neat GO or SA paper, X-ray photoelectron spectroscopy (XPS) analysis demonstrates that the C 1s components corresponding to C−OH, C−O−C, C═O, and O−C═O groups in the composite paper are slightly shifted from 285.5 (GO)/286.0 (SA), 286.8/287.0, 287.8, and 289.0 eV to 285.9, 287.2, 288.2, and 289.0 eV (Figure 2f), respectively, indicating the coordination/cooperation between oxygen-containing groups of both GO sheets and the SA biopolymer. Moreover, the relative areas of all peaks corresponding to oxygen-containing groups changed to some degree, in particular, the decrease of the O−C═O groups, supporting the hypothesis that the C−OH groups are generated by the double bond-opening reaction of the O−C═O group (Table S1).[34] More importantly, the layered GO/SA composites, by presenting higher-ordered structures, and the intercalation of SA biopolymers in the gallery spacing (d-spacing) of GO sheets changed regularly with d-spacing between the GO sheets, which was confirmed by the characteristic diffraction peak of X-ray diffraction (XRD) (Figure 2g and Figure S5a in SI).[35] The typical strong diffraction peak is usually assigned to stacks of hydrophilic regions with oxygenated functional groups on GO sheets. The d-spacing in the GO/SA composite paper has a nearly linear relationship with the GO volume content. The d-spacing of pure GO is about 9.0 Å ($2\theta = 9.8°$). For the GO/SA composite, the d-spacing of the GO sheets clearly decreases from approximately 8.6 Å ($2\theta = 10.2°$) for 13.5 vol % of GO content to ~7.9 Å
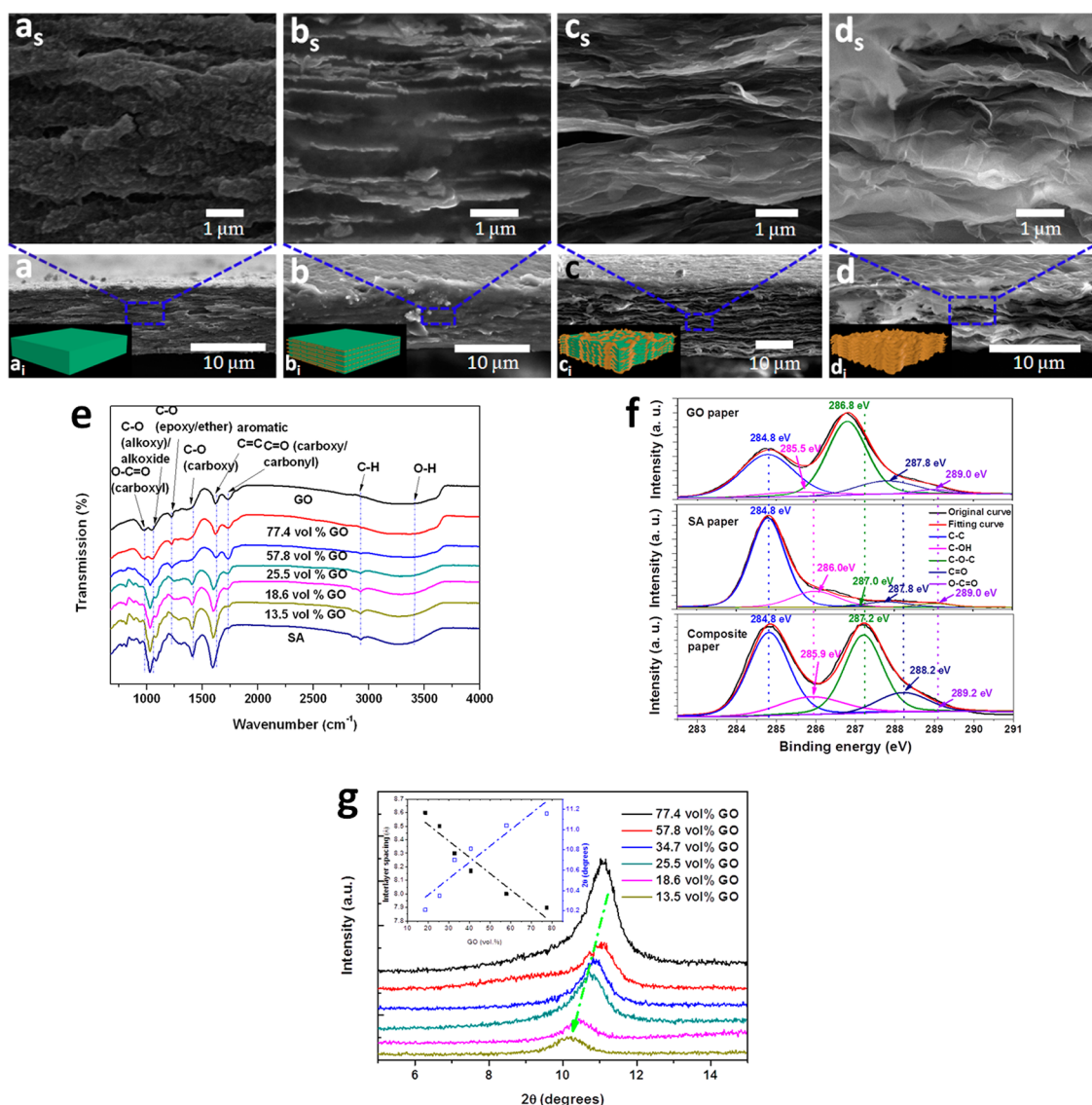
Figure 2. Comparison of cross-sectional morphology and structure of neat GO, SA, and the GO/SA composite papers. From top to bottom: High- and low-resolution SEM images (a_s−d_s and a−d) and schematic diagram (a_i−d_i) of neat SA, 18.6 vol % of GO composite paper, 56.3 vol % of GO composite paper, and pure GO paper, respectively. (e) Fourier transform infrared spectra for neat GO, SA, and the composite papers. (f) Deconvoluted C 1s X-ray photoelectron spectroscopy spectra of neat GO, SA, and the composite papers. The C 1s peak of the species can be fitted into five line shapes with binding energies at 284.8, 285.5−286.0, 286.8−287.2, 287.2−288.2, and 289.0 (289.2) eV, corresponding to the C−C/C=C, C−OH, C−O−C, C=O, and O−C=O, respectively. (g) X-ray diffraction patterns of the GO/SA composite papers. Plot of interlayer spacing and diffraction peak position are dependent as a function of GO concentration. The black dashed line represents a linear best fit to the data of the interlayer spacing, and the blue dashed line represents a linear best fit to the data of the diffraction peak.

($2\theta = 11.2°$) for 77.4 vol % of GO content, which is also strong evidence for the intercalation of the SA biopolymer into the d-spacing between GO sheets. For the initial d-spacing of 9.0 Å, the change is from 0.4 to 1.1 Å, which is much smaller than the van der Waals diameter of water, 2.82 Å.[35] Hence, we conjectured that due to the presence of the biopolymer "backbone" in the interlamination of GO nanosheets, like PVA, plenty of hydroxyl groups of the SA biopolymer form a H-bonding network with the GO sheets and then proceed to form a more stable arrangement than the homogeneous distribution of hydrogen bonds in the GO paper, offering a strong shared

cooperative mode of stress transfer on the GO/SA interface.[17]

The mechanical properties of the composite papers have been evaluated in the natural environment (25 °C, 15% RH) (Figure 3a−d and Supporting Information movies S1−S3). The GO/SA paper displays a perfect combination of high tensile strength and toughness (movie S1), greater than those of the neat GO or SA paper (see movies S2 and S3) or other binary composites. The ultimate strength reaches 272.3 ± 13.9 MPa (up to 286.2 MPa in some cases), with the ultimate toughness staying within 11.9 ± 0.6 MJ m^{-3}, and the toughness comes up to a very high value of
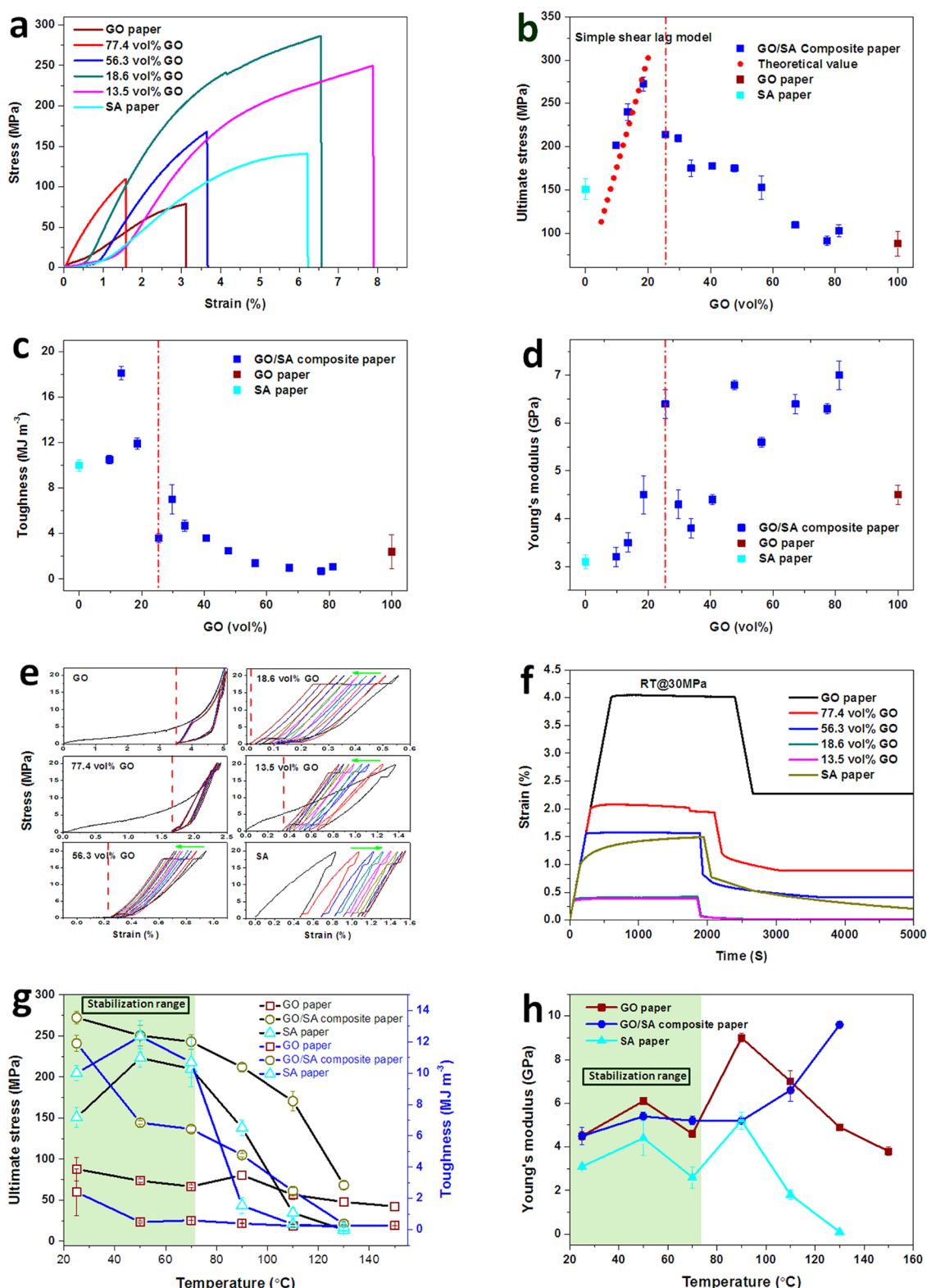
Figure 3. Mechanical properties of neat GO, SA, and the GO/SA composite papers in the natural environment (a–f)/annealed at various temperatures under ultrapure N$_2$ atmosphere (g,h). (a) Representative stress–strain data from the tensile test for the composite papers with different GO concentration. (b) GO concentration dependence of ultimate tensile strength. The red-filled circles in (b) represent the predicted tensile strength based on the shear lag model. (c) GO concentration dependence of the toughness. (d) GO concentration dependence of Young's modulus. (e) Stress–strain curves in cyclic loading experiments. (f) Typical creep and recovery curves. (g) Annealing temperature dependence of ultimate tensile strength and toughness. (h) Annealing temperature dependence of Young's modulus.

18.1 ± 0.6 MJ m^{-3} obtained in the composite paper. In addition, with the increase of their thickness, the mechanical properties of the paper maintain the outstanding values (Figure S5b). The ultimate strength increases linearly from 201.8 ± 1.6 MPa (9.8 vol %) to 272.3 ± 8.0 MPa (18.6 vol %) and then decreases gradually from 213.8 ± 2.2 MPa (25.5 vol %) to 102.8 ± 6.8 MPa (81.2 vol %). The changes of the toughness in the above range exhibit trends similar to those of the tensile strength. A comparison of our experimental values and theoretical predictions from the simplified shear lag model was made, and the results are pretty similar. For example, the ultimate strength in the range agrees well with the theoretical predictions which assume that the ultimate strength of GO sheets in the SA matrix is around 2.0 GPa (theoretical methods in SI).[1] Besides, compared to the stiffness (∼60 GPa) of natural nacre, the Young's modulus of the our composite paper is lower (4.6 ± 0.3 GPa), which can be attributed to massive ductile/soft SA biopolymer. However, the value is slightly higher than that of the neat GO (4.5 ± 0.2 GPa) or SA paper (3.1 ± 0.1 GPa), which is due to the network of H-bonding/cooperative interactions on the GO/SA interface, combined with the results of XRD patterns (Figure 2g). For a relative low GO content in the composite paper (9.7−25.5 vol %), the value increases gradually with the increment of GO concentration. However, it is also a fact that the experimental values are by far lower than the theoretical values predicted by the Halpin−Tsai laminated model for perfect orientation of 2D reinforcing sheets (Figure S6 in SI).[18] First, we consider that such variance can be attributed to the ideal applied model. In the estimation of the values of the Young's modulus for GO sheets and the SA biopolymer, there exists a difference between theory and practice. In particular, the ideal effective Young's modulus (207.6 ± 23.4 GPa) of an ideal monolayer GO sheet is likely much high than the realistic modulus,[24] as individual GO sheets in realistic test specimens always contain some defects, crumpled, folded, entangled with each other, leading to a relative low Young's modulus of an individual GO sheet. Second, such discrepancy arises not only from the "size-dependent effect" of the specimens but also from the variety of the hybrid GO/SA construction, interactions, and the possibility of rare but known GO/SA interphase reinforcement. Therefore, through analyzing the mechanical test results of our GO/SA composite paper, although the Young's modulus and toughness are obviously exclusive, the attainment of both strength and toughness achieve a vital requirement for most structural materials.

The stress−strain curve of the composite paper under cyclic loading exhibits consecutive enhancement of Young's modulus as the number of loading/unloading cycles increases. After eight cycles (0.001−20 MPa, keeping (1 s), and back at 50 μm min^{-1}),

the Young's modulus values of the composite paper (18.6 vol % of GO) are obviously higher (40−80% higher for modulus) than that of the species with one loading/unloading cycle (Figure 3e). In addition, the creep and recovery curves under the stress of 30 MPa further show that there is slight residual deformation after recovery, which indicates that the stronger load transfer and bonding capabilities can effectively restrain the slip between the two components; this hypothesis is consistent with the repeated cyclic loading experiments (Figure 3f). This result refers to recoverable H-bonding networks between hard GO sheets and a soft SA matrix in the composite paper. Instead, according to intrinsic toughening/strengthening mechanisms, the behavior based on the H-bonding networks essentially enhances the composite material's inherent damage resistance.

Additionally, combined with some related characterizations including XRD patterns, SEM images, and TG-DSC analysis, the mechanical properties of the nacre-like GO/SA composite paper in high relative humidity (>85% RH) (Figure S7) and annealed at various temperatures (from 50 to 150 °C) under ultrapure N$_2$ atmosphere (Figure 3g,h and Figure S8) have also been studied. As a comparison, the mechanical properties of these samples in the high RH of >85% are much lower than those of the samples in the natural environment. The effect of the humid atmosphere on the mechanical properties of nacre-like GO/SA paper can be due to a large number of water molecules on the GO/SA interface/between interlaminations, which results in the reduced H-bonding/cooperative interactions (the detailed discussion is shown in Figure S7). Moreover, the strength, toughness, and Young's modulus of pure GO, SA, and GO/SA composite papers are found to be dependent on the thermal annealing temperature, as shown in Figures 3g,h. Note that for three types of samples, the mechanical properties remain basically stable or reduce slightly when thermally annealed below 70 °C. With increasing temperature up to about 150 °C, both strength and toughness of pure GO paper still remains mostly unchangeable or reduces slightly, but for pure SA paper, these two values decrease gradually from 223.1 ± 11.2 MPa and 12.4 ± 1.0 MJ m^{-3} to 14.0 ± 2.0 MPa and 0.16 ± 0.01 MJ m^{-3}. Notably, as for pure SA paper, the mechanical property is clearly stronger at a properly annealed temperature (below 70 °C) than that in the natural environment. The enhancement may be attributed to the elimination of partial "free water" that exists among the SA biopolymer by thermal annealing, which leads to enhancement of the H-bonding contact and intermolecular interactions of the SA biopolymer.[35] However, the Young's modulus of pure GO and SA paper increases first (70−90 °C) and then decreases (90−150 °C) with the increment of thermal annealing temperature. For the GO/SA composite paper,
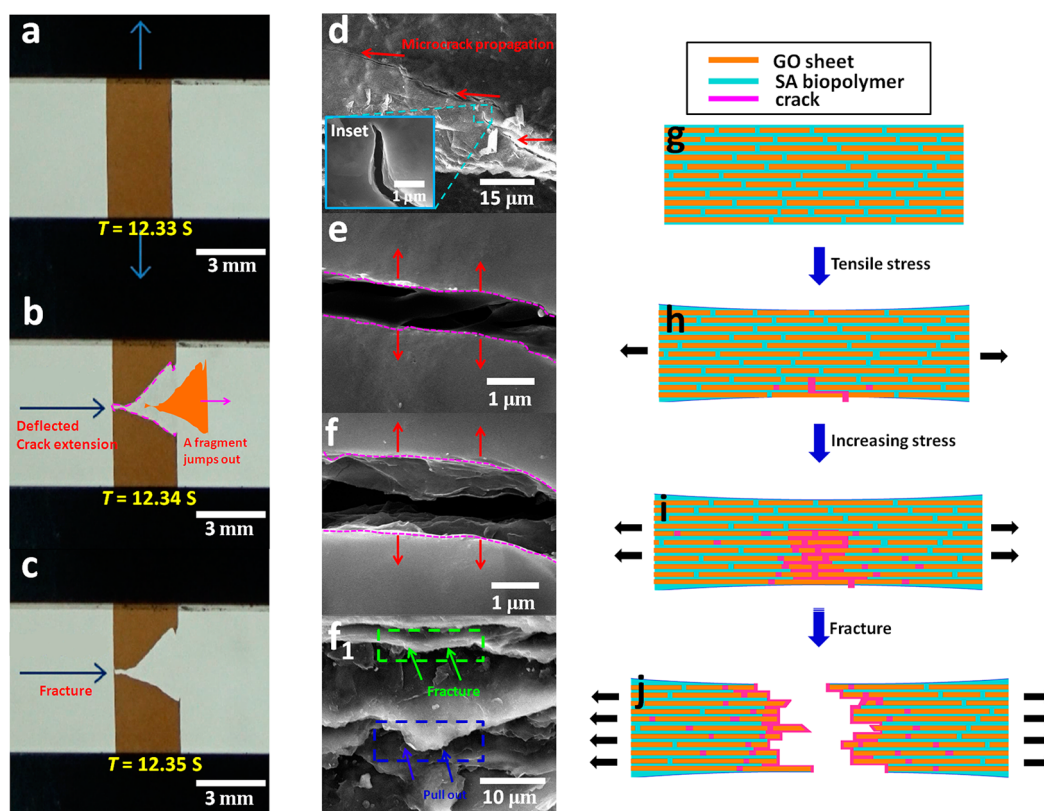
Figure 4. Digital photograph of rupture process by *in situ* tensile test (a−c) (see movie S1), fracture morphology (d−f), and proposed GO-sheet-reinforced (strengthening/toughening) mechanism (d−g) of the nacre-like composite paper (testing condition: 25 °C and 15% RH). (a) *In situ* tensile test of a sample (side view) at T = 12.34 s, with intact states. (b) At T = 12.35 s, the rupture occurs and, simultaneously, a fragment jumps out. (c) Small amount of time later (T = 12.35 s), complete rupture occurs. (d) Fracture surface of the nacre-like composite paper that exhibits long-range microcrack deflection. Inset: Amplifying microcrack propagation and fracture at the tip of the microcrack. (e) Microcrack extension on the composite surface, with the onset of microcrack branching and bridging/adhering by non-microcracked ligaments. Red arrows indicate the direction of the microcrack extension, and pink dotted lines represent the microcrack extension paths. (f) Complete fracture of the composite associated with GO sheet fracture/pull out. Note that the fracture/pull out (f_1) can further be observed in a green/blue dotted rectangular box, separately. (g) Simplified structural schematic diagram, showing well-aligned GO sheets surrounded by the SA matrix. (h) Under tensile stress, the GO sheets effectively transfer loading to the SA matrix and deflect the microcrack. (i) H-bonding/cooperative force on the GO/SA interface restricts sliding of GO sheets, which spread rapidly to other GO/SA interfacial layers, accompanied by further increased tensile stress. (j) Composite paper finally breaks under the GO sheets' fracture/pull out mode.

although both strength and toughness decrease gradually from 250.5 ± 12.3 MPa and 6.84 ± 0.1 MJ m^{-3} to 68.3 ± 4.2 MPa and 0.37 ± 0.15 MJ m^{-3}, the Young's modulus increases gently from 5.4 ± 0.4 to 9.6 ± 0.1 GPa with the increment of thermal annealing temperature. As a whole, below 110 °C, the mechanical property of the nacre-like composite paper is stronger than that of pure GO or SA paper. Combining the XRD and TG-DSC measurement results (Figure S8d−g), these results further demonstrate that water molecules in the composite play a significant role in adjusting the mechanical property. So, the reduction of both strength and toughness and the enhancement of Young's modulus when treated above 70−150 °C (Figure 3g) is due to as a sequence of water molecules from the loss of "free water" and partial "confined water" in the material.

On the basis of the above results of the mechanical properties under wet environment/thermal annealing

with different temperatures, the GO/SA composite paper is much more suitable for being used in the natural environment or below 70 °C, by holding the RH relatively low to keep the excellent mechanical performance. In order to reveal the strengthening and toughening mechanism of the binary synergy, rupture process and fracture morphology of the composite are carefully studied, as displayed in Figure 4a−f (see more details in movie S1). The composite paper could maintain the integrity after a period of stretching (T = 12.33 S), and some invisible microcracks at the edge of the sample appeared (Figure 4d). At T = 12.34 S, cracks propagated rapidly, and a fragment jumps out simultaneously (Figure 4b), and complete rupture occurred during a tiny instant (assuredly far less than 0.01 s, Figure 4c), indicating tortuous crack extension paths, crack deflection, and brittle rupture, which is absolutely different from the fracture feature of pure GO or SA paper (see movies S2 and S3). Moreover, at the

micrometer scale, some tortuous/long-range micro-crack paths emerge on the surface, and the amplified tip of microcracks is observed in the nacre-like paper by the SEM image (Figure 4d). During the microcrack extension, incomplete fracture and microcrack bridging/adhering are observed inside the microcrack (Figure 4e). As further microcrack extension, the complete rupture associated with GO sheet fracture/pull out is also seen in Figure 4f−f_i, which is also successfully predicted by simplified shear lag model (see SI for details). The feature of the fracture surface for the nacre-like composite paper is fully distinguished from that of pure GO or SA paper (Figure S9).

In terms of the strengthening effect, on the one hand, the GO/SA paper is structured hierarchically and actually consists of nanometer-sized GO/SA building blocks, providing a benefit from mechanical size effects (size-dependent strengthening). On the other hand, more interestingly, based on a shear model, combined with our experimental results (see Scheme S1 in SI),[36] we can successfully quantify the strength behavior of the unit cell in the composite paper. As a result, the practical shear stress (τ = 62.7 MPa) on the GO/SA interface, corresponding to the ultimate stress in our experiment, is consistent with the average shear stress (τ_{ave} = 63 MPa) by theoretical calculation, verifying the realization of the strengthening effect. Furthermore, by analyzing both intrinsic and extrinsic toughening of natural nacre and combining fracture morphology and the fracture process of the nacre-like composite (see movie S1), we infer that the GO/SA paper relies similarly on the toughening mechanism. On the scale of the ductile SA biopolymer macromolecules, intrinsic toughening (plasticity) is the primary source of fracture resistance through the mechanisms of molecular uncoiling and intermolecular sliding of molecules, akin to the nanometer size of dislocation of Burgers' vector in metals.[3] On the other hand, at micrometer-size scale, the principal sources of toughening are extrinsic and cause extensive crack deflection (the crack can be deflected around the GO/SA interface, requiring more energy to propagate than a straight crack) and crack bridging by uncracked ligaments (Figure 4b). Therefore, the reason for extrinsic toughening can be mainly due to the breaking of sacrificial bonds (H-bonding/cooperative interactions) that increased energy dissipation at the GO/SA interfaces. Finally, the tortuous crack path and pull out/fracture of GO sheets, with movie S1 in the SI showing the fracture of the composite paper in the environment at ordinary temperature (25 °C) and ordinary humidity (15% RH), further provide the major responsibility of both intrinsic and extrinsic toughening. Hence, the form of the hybrid GO/SA interfacial structure (the binary synergism) from stiff GO sheets as a filler/brick and soft/ductile SA biopolymer as a matrix/mortar is beneficial to realize the strengthening and toughening of the nacre-like composite.

By analyzing the fracture process and fracture morphologies of the composite paper as described above, combined with the strengthening/toughening mechanisms of biological composite materials (e.g., nacre, bone), we proposed a crack extension model to depict the binary synergistic strengthening/toughening effect, as shown in Figure 4g−j. First, a deflected/tortuous microcrack induced by a GO sheet adhered to the SA biopolymer, and a massive cooperative force including H-bonding and other intermolecular interactions on the interface can be restricted to the sliding of adjacent GO sheets (strain hardening, Figure 3g). Second, the increasing stress transferred to the vicinal region along the interfacial layer rapidly, which subsequently motivates the potential sliding of adjacent multiple layers (Figure 4h). Such microcrack deflection, strain hardening, and motivation of the potential sliding of multiple adjacent sliding sites are accumulated step-by-step until the materials fail under platelet fracture/pull out mode. Besides, from the nonlinear stress−strain curve (Figure 3a), the deformation process, possibly including viscoplastic and plastic deformation, demonstrated by the strain hardening, is similar to the deformation of hydrated nacre. Therefore, a large amount of the viscoplastic/plastic energy dissipation by the hybrid GO/SA layers in a synergy pervades through the full specimen, rather than only on the fracture surface.

Figure 5 summarizes the natural environment mechanical performance of the GO- and SA-related papers from the literature. The ultimate stress (286.2 MPa) of our nacre-like paper is approximately 2−3-fold higher than that of natural nacre (80−135 MPa), bone (150 MPa), and dentin (105 ± 16.4 MPa). The highest measured toughness is up to 18.1 ± 0.6 MJ m^{-3}, which is more than 10 times higher than that of the natural nacre, 15 times higher than that of the bone, and over 9 times higher than that of the dentin. Also, the tensile strength and toughness are many-fold (10−20) higher than those of the SA/PEO nanocomposite fibers[37] and are obviously higher than those of the SA/SWCNT fibers,[28] respectively. In addition, the ultimate stress is 1.5−14 times higher than those for most of the composite materials containing GO sheets, and the toughness is also many-fold (2−100) higher.[13,14,38−40] For instance, although the GO/silk nanocomposite shows very high strength of 330 MPa, its toughness is only 3.4 MJ m^{-3}.[2] Moreover, GO/PAA shows a considerably high toughness of 9.8 MJ m^{-3}, and their value of ultimate stress is very low due to a weak poly-(ε-caprolactone) matrix.[41] However, the Young's modulus of the nacre-like GO/SA paper is lower than that of most GO- and SA-related papers, which can be attributed to the intrinsic property/feature (low modulus and high ductility) of the SA polysaccharide biopolymer, which is a large proportion of the composite. Despite its own relative low Young's modulus, the
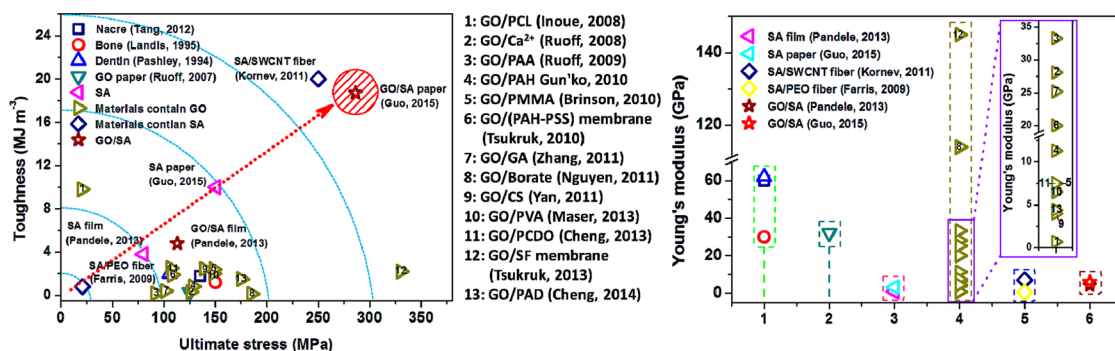
Figure 5. Comparison of mechanical properties among GO- and SA-related papers in the natural environment. All of data for the materials were taken from the respective papers that provide the ultimate stress, toughness, and Young's modulus. The arrow displays the overall desired direction for the composite reinforcement. (*Abbreviations (see SI for details). **Reference: nacre,[8] bone,[42] dentin,[43] GO paper,[44] SA film,[45] GO/PCL,[46] GO/Ca^{2+},[34] GO/PAA,[41] GO/PAH,[47] GO/PMMA,[15] GO/(PAH−PSS) membrane,[18] GO/GA,[30] GO/borate,[15] GO/CS,[48] GO/PVA,[49] GO/PCDO,[21] GO/SF membrane,[2] GO/PDA.[50])

nacre-like GO/SA composite paper can achieve excellent strength and toughness, and this material still has a great potential advantage of being applied in engineering materials in order to prevent catastrophic fracture.

CONCLUSION

Taken all together, by mimicking the hybrid structure of natural nacre, we successfully fabricated a kind of nacre-like GO/SA composite paper. The binary synergistic strengthening/toughening enhancement from both components with a complementary heterogeneous nature of abundant oxygen-containing functional groups on their surfaces was promoted by strong cooperative/H-bonding interactions that participated in the interfacial bonding of the composite paper. Importantly, it exhibited a unique combination of high strength (272.3 ± 13.9 MPa) and toughness

(12.5 MJ m^{-3}, up to 18.1 ± 0.6 MJ m^{-3} in some cases), by far superior to that of all natural nacre and other binary GO- and SA-related composites. In addition, by analyzing the failure behavior, we found that it strongly depends on the interface strengthening and both the intrinsic and extrinsic toughening mechanism. Notably, accompanying a thickness increase, the mechanical performance of the paper still remains relatively stable and maintains its outstanding mechanical performance in an environment below 70 °C and with relatively low RH.

Due to the outstanding mechanical properties, fast fabrication, controlled permeability, and natural biocompatibility, the nacre-like GO/SA composite paper will be beneficial for potential applications, such as biosensing devices, scaffolds, nanoporous biological and chemical filters, and permeable membranes for separation and delivery.

EXPERIMENTAL SECTION

Preparation of Graphene Oxide, Sodium Alginate, and Composite Dispersions. Graphene oxide was prepared from graphite powder by the modified Hummers method. Briefly, graphite powder (3.0 g) was vigorously stirred with a blend of concentrated H_2SO_4 (120 mL) and $KMnO_4$ (15 g) below 20 °C for 20 h to yield GO (see SI for synthetic details). Colloidal GO dispersion was prepared following a reported literature protocol by suspending the as-prepared GO in water and sonicating for 60 min. This dispersion was purified *via* centrifugation (see SI for synthetic details). Complete exfoliation of GO into GO sheets in the dispersion was demonstrated by the absence of a diffraction peak in the PXRD pattern, the characterized G and D bands in the Raman spectrum, and the individual GO sheets of AFM images. Aqueous SA solution was obtained by adding the SA biopolymer into deionized water, which was stirred for 60 min to dissolve fully. Composite dispersions of GO and SA were prepared by incorporating a colloidal GO dispersion (1 mg mL^{-1}) into an aqueous solution of SA (0.3 wt %).

Fabrication of Graphene Oxide, Sodium Alginate, and GO/SA Composite Papers. GO, SA, and GO/SA composite papers were prepared by filtering the diluted colloidal GO dispersions, aqueous SA solution, or composite dispersions, respectively, through a CN-CA mixed cellulose filter membrane. A series of GO/SA composite papers with different GO concentrations could be obtained by

tuning the volume ratios of colloidal GO dispersions to the aqueous SA solution. A water circulation multifunction vacuum pump with a vacuum filter holder was utilized for vacuum filtration. After filtration, specimens were air-dried until they could be peeled off the paper for analysis.

Thermal Annealing Treatment of Graphene Oxide, Sodium Alginate, and GO/SA Composite Papers. GO, SA, and GO/SA composite papers were thermally annealed at different temperatures (50−150 °C) by a SK-G10123K pipe furnace (Tianjin Zhonghuan Lab Furnace Co., Ltd.) in a 50 mL min^{-1} flow of 99.9995% N_2 atmosphere for 2 h prior to the measurements.

Characterization. The tensile mechanical properties were measured using a Shimadzu AGS-X tester with a dynamic mechanical analyzer. Static tensile tests were evaluated at a load speed of 1 mm min^{-1} with a gauge length of 5 mm. Short time creep tests were conducted in the tensile mode at 27 °C with an applied stress of 30 MPa and a ramp rate of 20 μm min^{-1}, and the creep strain was determined as a function of time (when tensile stress was up to 30 MPa, kept for 30 min, and then deformation recovery, waiting for 60 min). The cyclic tensile tests were monitored with a preload of 0.01 N for 2 h at 27 °C, a tensile stress of 20 MPa kept for 1 s, and a ramp rate of 50 μm min^{-1} for eight cycles. A humidifier was used to maintain high relative humidity (>85% RH) in order to carry out the *in situ* tensile test of the samples with a load speed of 500 μm min^{-1} with a gauge length of 5 mm. All of the papers were cut into strips with

a length of 20 mm and a width of 3 mm. The specimen thickness was obtained from the SEM image of the fracture edges.

SEM images were taken by the Quanta 250 FEG. AFM was performed by a Bruker Dimension Icon to obtain the rms roughness and topography. All of the XPS measurements were taken in an ESCALab220i-XL (Thermo Scientific) using a monochromatic Al Kα X-ray source. Raman spectroscopy measurements were carried out using a LabRAM HR800 (Horiba Jobin Yvon) with a 514 nm wavelength incident laser. FTIR spectra were collected using a Thermo Nicolet nexus-470 FTIR instrument. UV−vis spectrum was taken by a UV−vis−NIR spectrophotometer (UV-3600, Shimadzu). Thermogravimetric (TG) analysis was performed on a TG/DSC, NETZSCH STA 449F3, under N_2 at a temperature increasing rate of 10 °C min^{-1}.

Conflict of Interest: The authors declare no competing financial interest.

Supporting Information Available: Materials and detailed experimental methods for the synthesis of GO, Raman of GO sheets, AFM images of individual GO sheets, cross-sectional SEM images, XRD, XPS, TG-DSC analysis, the mechanical properties under wet environment, theoretical methods, and some movies of the fracture behaviors of the samples under tensile tests. The Supporting Information is available free of charge on the ACS Publications website at DOI: 10.1021/acsnano.5b02333.

REFERENCES AND NOTES

1. Bonderer, L. J.; Studart, A. R.; Gauckler, L. J. Bioinspired Design and Assembly of Platelet Reinforced Polymer Films. *Science* **2008**, *319*, 1069–1073.
2. Hu, K.; Gupta, M. K.; Kulkarni, D. D.; Tsukruk, V. V. Ultra-Robust Graphene Oxide-Silk Fibroin Nanocomposite Membranes. *Adv. Mater.* **2013**, *25*, 2301–2307.
3. Ritchie, R. O. The Conflicts between Strength and Toughness. *Nat. Mater.* **2011**, *10*, 817–822.
4. Espinosa, H. D.; Rim, J. E.; Barthelat, F.; Buehler, M. J. Merger of Structure and Material in Nacre and Bone-Perspectives on De Novo Biomimetic Materials. *Prog. Mater. Sci.* **2009**, *54*, 1059–1100.
5. Fang, Z.; Zhu, H.; Yuan, Y.; Ha, D.; Zhu, S.; Preston, C.; Chen, Q.; Li, Y.; Han, X.; Lee, S.; et al. Novel Nanostructured Paper with Ultrahigh Transparency and Ultrahigh Haze for Solar Cells. *Nano Lett.* **2014**, *14*, 765–773.
6. Fratzl, P.; Weinkamer, R. Nature's Hierarchical Materials. *Prog. Mater. Sci.* **2007**, *52*, 1263–1334.
7. Meyers, M. A.; Chen, P. Y.; Lin, A. Y. M.; Seki, Y. Biological Materials: Structure and Mechanical Properties. *Prog. Mater. Sci.* **2008**, *53*, 1–206.
8. Wang, J.; Cheng, Q.; Tang, Z. Layered Nanocomposites Inspired by the Structure and Mechanical Properties of Nacre. *Chem. Soc. Rev.* **2012**, *41*, 1111–1129.
9. Bouville, F.; Maire, E.; Meille, S.; Van de Moortèle, B.; Stevenson, A. J.; Deville, S. Strong, Tough and Stiff Bio-inspried Ceramics from Brittle Constituents. *Nat. Mater.* **2014**, *13*, 508–514.
10. Mirkhalaf, M.; Dastjerdi, A. K.; Barthelat, F. Overcoming the Brittleness of Glass through Bio-Inspiration and Micro-Architecture. *Nat. Commun.* **2014**, *5*, 1–9.
11. Li, Y. Q.; Yu, T.; Yang, T. Y.; Zheng, L. X.; Liao, K. Bio-Inspired Nacre-Like Composite Films based on Graphene with Superior Mechanical, Electrical, and Biocompatible Properties. *Adv. Mater.* **2012**, *24*, 3426–3431.
12. Tang, Z.; Kotov, N. A.; Magonov, S.; Ozturk, B. Nanostructured Artificial Nacre. *Nat. Mater.* **2003**, *2*, 413–418.
13. Potts, J. R.; Dreyer, D. R.; Bielawski, C. W.; Ruoff, R. S. Graphene-Based Polymer Nanocomposites. *Polymer* **2011**, *52*, 5–25.
14. Das, P.; Schipmann, S.; Malho, J. M.; Zhu, B.; Klemradt, U.; Walther, A. Facile Access to Large-Scale, Self-Assembled, Nacre-Inspired, High-Performance Materials with Tunable Nanoscale Periodicities. *ACS Appl. Mater. Interfaces* **2013**, *5*, 3738–3747.
15. An, Z.; Compton, O. C.; Putz, K. W.; Brinson, L. C.; Nguyen, S. T. Bio-Inspired Borate Cross-Linking in Ultra-Stiff Graphene Oxide Thin Films. *Adv. Mater.* **2011**, *23*, 3842–3846.
16. Putz, K. W.; Compton, O. C.; Palmeri, M. J.; Nguyen, S. T.; Brinson, L. C. High-Nanofiller-Content Oxide-Polymer Nanocomposites *via* Vacuum-Assisted Self-Assembly. *Adv. Funct. Mater.* **2010**, *20*, 3322–3329.
17. Compton, O. C.; Cranford, S. W.; Putz, K. W.; An, Z.; Brinson, L. C.; Buehler, M. J.; Nguyen, S. T. Tuning the Mechanical Properties of Graphene Oxide Paper and Its Associated Polymer Nanocomposites by Controlling Cooperative Intersheet Hydrogen Bonding. *ACS Nano* **2012**, *6*, 2008–2019.
18. Kulkarni, D. D.; Choi, I.; Singamaneni, S. S.; Tsukruk, V. V. Graphene Oxide-Polyelectrolyte Nanomembranes. *ACS Nano* **2010**, *4*, 4667–4676.
19. Mirkhalaf, M.; Dastjerdi, A. K.; Barthelat, F. Overcoming the Brittleness of Glass through Bio-Inspiration and Micro-Architecture. *Nat. Commun.* **2014**, *5*, 1–9.
20. Podsiadlo, P.; Kaushik, A. K.; Arruda, E. M.; Waas, A. M.; Shim, B. S.; Xu, J.; Nandivada, H.; Pumplin, B. G.; Lahann, J.; Ramamoorthy, A.; et al. Ultrastrong and Stiff Layered Polymer Nanocomposites. *Science* **2007**, *318*, 80–83.
21. Cheng, Q.; Li, M.; Jiang, L.; Tang, Z. Bioinspired Layered Composites Based on Flattened Double-Walled Carbon Nanotubes. *Adv. Mater.* **2012**, *24*, 1838–1843.
22. Cheng, Q.; Wu, M.; Li, M.; Jiang, L.; Tang, Z. Ultratough Artificial Nacre based on Conjugated Cross-Linked Graphene Oxide. *Angew. Chem., Int. Ed.* **2013**, *52*, 3750–3755.
23. Yao, H. B.; Ge, J.; Mao, L. B.; Yan, Y. X.; Yu, S. H. 25th Anniversary Article: Artificial Carbonate Nanocrystals and Layered Structural Nanocomposites Inspired by Nacre: Synthesis, Fabrication and Applications. *Adv. Mater.* **2014**, *26*, 163–188.
24. Suk, J. W.; Piner, R. D.; An, J.; Ruoff, R. S. Mechanical Properties of Monolyer Graphene Oxide. *ACS Nano* **2010**, *4*, 6557–6564.
25. Medhekar, N. V.; Ramasubramaniam, A.; Ruoff, R. S.; Shenoy, V. B.; Shenoy, V. B. Hydrogen Bond Networks in Graphene Oxide Composite Paper: Structure and Mechanical Properties. *ACS Nano* **2010**, *4*, 2300–2306.
26. Bhattarai, N.; Li, Z.; Edmondson, D.; Zhang, M. Alginate-Based Nanofibrous Scaffolds: Structural, Mechanical, and Biological Properties. *Adv. Mater.* **2006**, *18*, 1463–1467.
27. Rosilo, H.; Kontturi, E.; Seitsonen, J.; Kolehmainen, E.; Ikkala, O. Transition to Reinforced State by Percolating Domains of Intercalated Brush-Modified Cellulose Nanocrystals and Poly(butadiene) in Cross-Linked Composites based on Thiol-Ene Click Chemistry. *Biomacromolecules* **2013**, *14*, 1547–1554.
28. Sa, V.; Kornev, K. G. A Method for Wet Spinning of Alginate Fibers with A High Concentration of Single-Walled Carbon Nanotubes. *Carbon* **2011**, *49*, 1859–1868.
29. Hummers, W. S.; Offeman, R. E. Preparation of Graphitic Oxide. *J. Am. Chem. Soc.* **1958**, *80*, 1339–1339.
30. Gao, Y.; Liu, L.; Zu, S.; Peng, K.; Zhou, D.; Han, B. H.; Zhang, Z. The Effect of Interlayer Adhesion on the Mechanical Behaviors of Macroscopic Graphene Oxide Papers. *ACS Nano* **2011**, *5*, 2134–2141.
31. Kudin, K. N.; Ozbas, B.; Schniepp, H. C.; Prud'homme, R. K.; Aksay, I. A.; Car, R. Raman Spectra of Graphite Oxide and Functionalized Graphene Sheets. *Nano Lett.* **2008**, *8*, 36–41.
32. Zhu, Y.; James, D. K.; Tour, J. M. New Routes to Graphene, Graphene oxide and Their Related Applications. *Adv. Mater.* **2012**, *24*, 4924–55.
33. Li, H.; Pang, S.; Wu, S.; Feng, X.; Mullen, K.; Bubeck, C. Layer-By-Layer Assembly and UV Photoreduction of Graphene-Polyoxometalate Composite Films for Electronics. *J. Am. Chem. Soc.* **2011**, *133*, 9423–9429.
34. Park, S.; Lee, K.-S.; Bozoklu, G.; Cai, W.; Nguyen, S. T.; Ruoff, R. S. Graphene Oxide Papers Modified by Divalent

Ions-Enhancing Mechanical Properties *via* Chemical Cross-Linking. *ACS Nano* **2008**, *2*, 572–578.

35. Zhu, J.; Zhang, H.; Kotov, N. A. Thermodynamic and Structural Insights into Nanocomposites Engineering by Comparing Two Materials Assembly Techniques for Graphene. *ACS Nano* **2013**, *7*, 4818–4829.

36. Barthelat, F.; Rabiei, R. Toughness Amplification in Natural Composites. *J. Mech. Phys. Solids* **2011**, *59*, 829–840.

37. Moon, S.; Ryu, B.-Y.; Choi, J.; Jo, B.; Farris, R. J. The Morphology and Mechanical Properties of Sodium Alginate based Electrospun Poly (Ethylene Oxide) Nanofibers. *Polym. Eng. Sci.* **2009**, *49*, 52–59.

38. Cheng, Q.; Jiang, L.; Tang, Z. Bioinspired Layered Materials with Superior Mechanical Performance. *Acc. Chem. Res.* **2014**, *47*, 1256–1266.

39. Liu, R.; Liang, S.; Tang, X. Z.; Yan, D.; Li, X.; Yu, Z. Z. Tough and Highly Stretchable Graphene Oxide/Polyacrylamide Nanocomposite Hydrogels. *J. Mater. Chem.* **2012**, *22*, 14160–14167.

40. Morimune, S.; Nishino, T.; Goto, T. Ecological Approach to Graphene Oxide Reinforced Poly (Methyl Methacrylate) Nanocomposites. *ACS Appl. Mater. Interfaces* **2012**, *4*, 3596–3601.

41. Park, S.; Dikin, D. A.; Nguyen, S. T.; Ruoff, R. S. Graphene Oxide Sheets Chemically Cross-Linked by Polyallylamine. *J. Phys. Chem. C* **2009**, *113*, 15801–15804.

42. Landis, W. J.; Librizzi, J. J.; Dunn, M. G.; Silver, F. H. A study of the Relationship between Mineral Content and Mechanical Properties of Turkey Gastrocnemius Tendon. *J. Bone Miner. Res.* **1995**, *10*, 859–867.

43. Sano, H.; Ciucchi, B.; Matthews, W. G.; Pashley, D. H. Tensile Properties of Mineralized and Demineralized Human and Bovine Dentin. *J. Dent. Res.* **1994**, *73*, 1205–1211.

44. Dikin, D. A.; Stankovich, S.; Zimney, E. J.; Piner, R. D.; Dommett, G. H.; Evmenenko, G.; Nguyen, S. T.; Ruoff, R. S. Preparation and Characterization of Graphene Oxide Paper. *Nature* **2007**, *448*, 457–460.

45. Ionita, M.; Pandele, M. A.; Iovu, H. Sodium Alginate/ Graphene Oxide Composite Films with Enhanced Thermal and Mechanical Properties. *Carbohydr. Polym.* **2013**, *94*, 339–344.

46. Kai, W.; Hirota, Y.; Hua, L.; Inoue, Y. Thermal and Mechanical Properties of A Poly(ϵ-Caprolactone)/Graphite Oxide Composite. *J. Appl. Polym. Sci.* **2008**, *107*, 1395–1400.

47. Satti, A.; Larpent, P.; Gun'ko, Y. Improvement of Mechanical Properties of Graphene Oxide/Poly(Allylamine) Composites by Chemical Crosslinking. *Carbon* **2010**, *48*, 3376–3381.

48. Han, D.; Yan, L.; Chen, W.; Li, W. Preparation of Chitosan/ Graphene Oxide Composite Film with Enhanced Mechanical Strength in the Wet State. *Carbohydr. Polym.* **2011**, *83*, 653–658.

49. Cano, M.; Khan, U.; Sainsbury, T.; O'Neill, A.; Wang, Z.; McGovern, I. T.; Maser, W. K.; Benito, A. M.; Coleman, J. N. Improving the Mechanical Properties of Graphene Oxide based Materials by Covalent Attachment of Polymer Chains. *Carbon* **2013**, *52*, 363–371.

50. Cui, W.; Li, M.; Liu, J.; Wang, B.; Zhang, C.; Jiang, L.; Cheng, Q. A Strong Integrated Strength and Toughness Artificial Nacre Based on Dopamine Cross-Linked Graphene Oxide. *ACS Nano* **2014**, *8*, 9511–9517.